Highly Ordered Helical Nanofilament Assembly Aligned by a Nematic Director Field

Fumito Araoka, Go Sugiyama, Ken Ishikawa, and Hideo Takezoe*

Successful alignment control of the B4 helical nanofilament assembly in a binary mixture system of bent-shaped and rod-shaped liquid crystals is demonstrated. The aligned nanofilament domains appear as extremely smooth and uniform stripes over millimeters. The interferometric second-harmonic generation microscopy technique is developed and applied to these aligned domains. It is found that not only chirality, but also polarity, are preserved in a single domain formed from a single nucleus. Such an easily processed uniform bulk of the spontaneously symmetry-broken material is intriguing in functional materials science.

1. Introduction

Although more than a dozen of years have passed since the discovery of the polar switching in the bent-shaped molecular system, it has still been generating much interest in the field of liquid crystals (LCs).[1,2] Particular attention has been paid to the physical and chemical characteristics of the chiral and polar states such as B2 and B4 phases: macroscopic polar domains and chiral domains arise through the symmetry breaking in achiral molecular systems, and in many cases the resultant chirality and polarity are mutually correlated.[3–5] Couples of years ago, Hough et al. clearly proved by electron diffraction (ED) and freeze fracture transmission electron microscopy (FFTEM) that a helical nanofilament bundle is the essential structure of the B4 phase.[6] Following this result, nano-segregated state in the binary mixture system of bent-shaped and rod-shaped molecules was extensively studied.[7–9] Particularly, we reported huge enhancement of optical activity observed as circular dichroism (CD) and optical rotation (OR) in the binary mixture system of the achiral bent-shaped (P-8-OPIMB: 1,3-phenylene bis[4-(4-octyloxyphenyliminomethyl)-benzoate], hereafter P8) and rod-shaped (5CB: 4-cyano-4′-n-pentyl-biphenyl) molecules originated from 5CB molecules in the nematic (N) phase segregated from the helical nanofilament network of P8.[7,8] In this case, 5CB molecules embedded in the B4 network are obviously affected by the chirality of the helical nanofilaments as inferred in the CD/OR signals. Thus, surely some kinds of chiral superstructures must be formed by 5CB molecules as the growth of nematic order is influenced by the chiral field of the surrounding B4 helical nanofilaments.[7,8]

Then, one question arises: What will happen if helical nanofilaments grow in the nematic director field? In the P8/5CB system, P8 nanofilaments are formed in the isotropic 5CB, and develop into the random network in the B4 phase. Upon further cooling, the expelled 5CB molecules take the transition to the nematic phase, so that the nematic director can be affected by the surrounding helical nanofilaments. Therefore, it is very natural to come to the idea that if homogeneous nematic alignment is first generated in a rubbing cell before the creation of the B4 nuclei, elongation of the B4 helical nanofilaments would progress along the nematic director to provide minimal distortion. Then, uniform alignment of the helical nanofilament assembly would be possible. Recently, Yoon et al. succeeded in uniformly aligning the nanofilaments by restricting its elongation in thin microchannels.[10] However, in their case, air flow is required to continuously apply a shear force. In this study, we demonstrate the realization of large uniform domains of aligned helical nanofilaments. Controlling and assembling self-organized functional molecules using such a mesoscopic state are an attractive subject for tailoring functional materials.[11–13] Indeed, it is one of enthusiastically studied topics in the field of materials science.

2. Results and Discussions

2.1. Chiral Segregation Observed using POM and CD in Nonrubbed Cells

A nematic (rod-shaped) LC used for this study must have a sufficiently wide nematic temperature range to include the temperature region of the B4 formation. In this study, 5PCB (4′-cyano-(1,1′-biphenyl)-4-yl-4-pentylbenzoate, chemical structure shown in **Figure 1**) was chosen and synthesized as such a LC molecule, instead of 5CB in the previous study.[8,9] The phase sequence of 5PCB on cooling is given as Iso;240 °C;N;51 °C;Cr by differential scanning calorimetry (DSC). As for a bent-shaped component, P8 whose phase sequence is Iso;174 °C;B2;152 °C;B3;140 °C;B4, was used as before. Figure 1 is a phase diagram of a P8/5PCB binary

Dr. F. Araoka, G. Sugiyama, Prof. K. Ishikawa, Prof. H. Takezoe
Department of Organic and Polymeric Materials
Graduate School of Science and Engineering
Tokyo Institute of Technology
2-12-1 O-okayama, Meguro, Tokyo 152-8552
E-mail: araoka.f.aa@m.titech.ac.jp

DOI: 10.1002/adfm.201201889

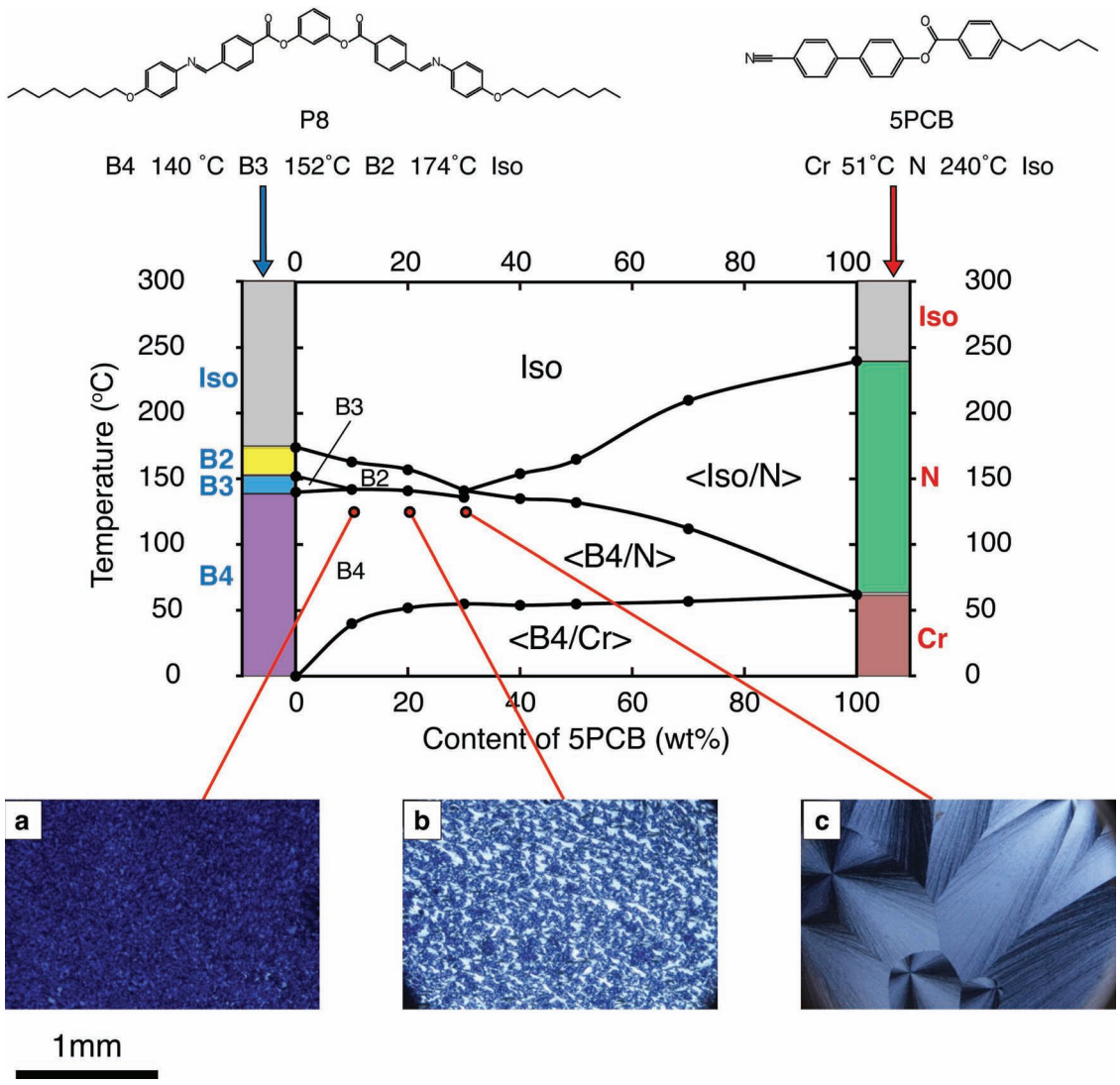

Figure 1. Phase diagram of the P8/5PCB mixture system. Chemical structures of P8 and 5PCB are also shown at the top. a–c) Microphotographs of POM textures of the <B4/N> phase at three different 5PCB contents. a) 10 wt%, b) 20 wt%, and c) 30 wt% at 120 °C.

mixture system determined by polarizing microscopy (POM) and DSC. Here nanophase-separated states are abbreviated to <P8/5PCB> (for example, <Iso/N> represents P8 in the Iso phase and 5PCB in the N phase). Similarly to the P8/5CB system, 5PCB content readily destabilizes B3 and B2 phases, and hence these phases appear only in the low 5PCB content region. In the higher content region above 30 wt%, a schlieren texture was observed by cooling from the Iso phase. In this state, 5PCB is in the N phase and P8 in the Iso phase, i.e., the <Iso/N> state. Further cooling yields relatively-smooth and highly-birefringent fan-shaped domains just below the <Iso/N> temperature, as shown in Figure 1c. Since this texture resembles the <B4/N> texture previously observed in the P8/5CB system, the state is considered to be <B4/N>. Textures of the <B4/N> state are also displayed in Figure 1a–c for comparison among three different 5PCB contents, a) 10, b) 20, and c) 30 wt% at 120 °C. In a 20 wt% 5PCB sample, still the birefringent texture of the nano-segregated domains can be observed. However in a 10 wt% 5PCB sample, it turns to a glassy and vivid blue texture of the typical B4 domains. All these mixtures show a highly birefringent crystalline phase below the <B4/N> temperature.

In the <B4/N> state, optical segregation of enantiomeric domains is recognizable by slightly uncrossing polarizers as shown in **Figure 2**a–c. Each domain has a certain single chirality. Figure 2d is a temperature dependence of a CD spectrum taken from a single domain of a 50 wt% 5PCB sample upon cooling from the Iso phase at a cooling rate of 5 °C/min. Initially in the Iso and <Iso/N> states, no CD signal could be observed since the molecules themselves were not chiral. However, immediately after entering <B4/N>, the CD signal appeared and exceeded over the maximum measurable limit of the CD spectrometer because of the formation of helical nanofilaments of P8. Its spectral shape is similar to that of B4 or <B4/Iso> rather than the <B4/N> of the P8/5CB system. In other words, the

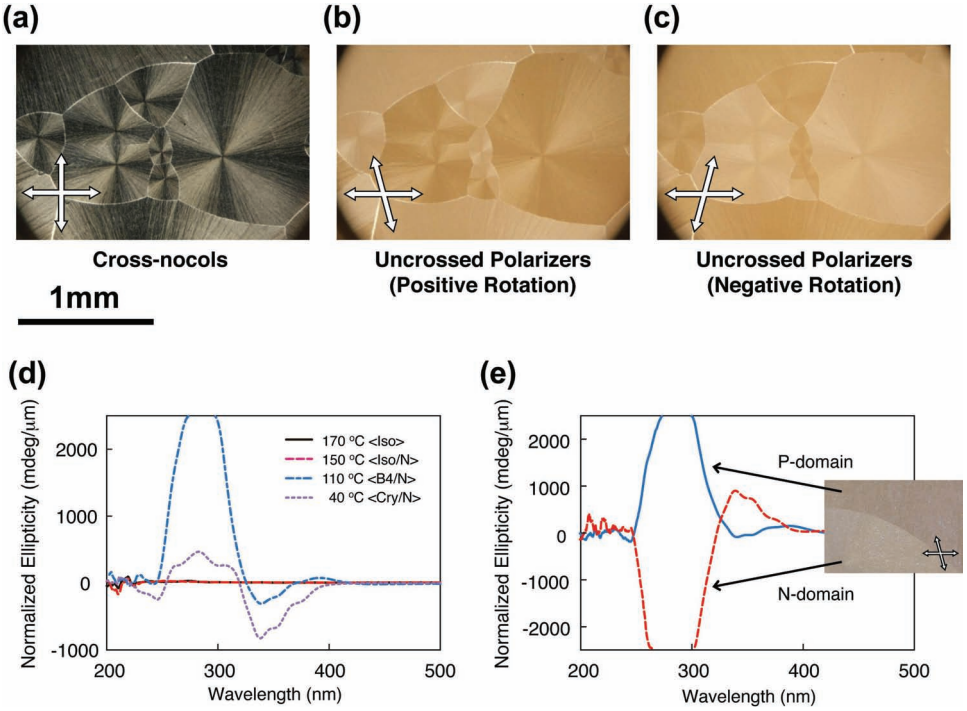

Figure 2. POM Textures in the <B4/N> phase of 50 wt% 5PCB sample at 120 °C under a) crossed and b,c) uncrossed polarizers. Each single domain has own single chirality. d) Temperature variation of the CD spectra of 50 wt% 5PCB mixture. e) Symmetric CD spectra measured for enantiomeric domains.

signal seems to originate from nanofilaments of P8. However, its peak magnitude is much higher than that estimated from the P8 fraction (730 mdegree/μm). Therefore, even though the main origin is the helical nanofilament P8, there is considerable contribution from the associated superhelical structure formed by the nematic 5PCB molecules, similar to the P8/5CB system. Besides, symmetric spectra were also confirmed for enantiomeric domains in the <B4/N> state, as shown in Figure 2e. In the growth process, the helical nanofilaments develop radially from its nucleus. Since the twist of the nanofilaments is a consequence of the layer chirality resulting from the correlation among a molecular permanent dipole, a molecular long axis, and a tilt of the bent-shaped molecules,[3] the chirality in these B4 domains is predetermined by each nucleus and preserved through the growth process.[14] In addition, each helical nanofilament owns spontaneous polarization along its longitudinal (helical) axis. Therefore, in these radial domains such as ones shown in Figure 2a, spontaneous polarization directs radially around the center of the Maltese-cross structures.

2.2. Orientation Control of Nanofilament in Rubbed Ultrathin Cells

Based on the above phase diagram, we chose the 50 wt% 5PCB mixture as a sample for the alignment control of the nanofilaments, since it has the <Iso/N> state with a sufficiently wide temperature range and the <B4/N> just below it. The sample mixture was injected into an ultrathin cell treated with antiparallel rubbing. By cooling from the Iso phase, we could obtain the <Iso/N> phase aligned uniformly along the rubbing direction. Further gentle cooling at a cooling rate slower than 0.5 °C/min brings about the huge growth of chiral fan-shaped domains in the <B4/N> state as shown in **Figure 3**. These chiral domains have an unusual four-brush pattern distinct

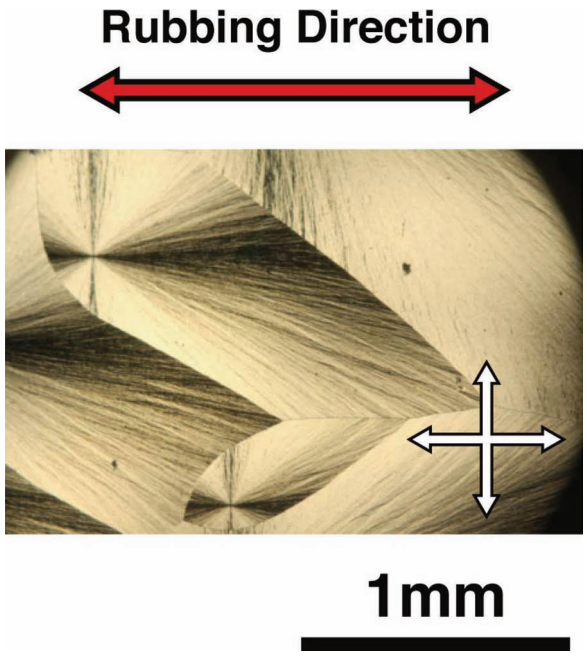

Figure 3. Large <B4/N> domains of a 50 wt% 5PCB mixture obtained in a rubbed ultrathin cell.

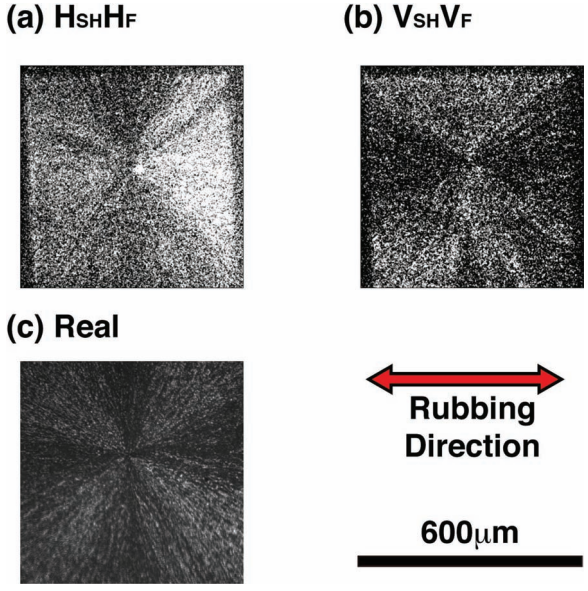

Figure 4. a,b) SH microscopy images of a <B4/N> domain in the rubbed ultrathin cell: a) $H_{SH}H_F$ and b) $V_{SH}V_F$ polarization combinations. c) The corresponding real image.

from the usual radial domains, i.e., when the rubbing direction is set along the polarizer axis, perfect extinction appears along the rubbing direction, but the orthogonal extinction becomes thin. Thus, there exists an obvious effect of the nematic director field.

From the POM observations on the <B4/N> domains, we know that each domain nucleated from each center of the four-brush patterns has a single chirality. Next question is the directional sense of the polar order (nanofilaments). To answer this question, second-harmonic generation (SHG) provides us with a powerful probe.[15,16] In the present study, SHG microscopy including interferometry was employed (details are described in the Experimental Section). **Figure 4**a,b are $H_{SH}H_F$ and $V_{SH}V_F$ SHG microscope images taken for a fan-shaped domain in the above rubbed ultrathin cell, together with the corresponding real image (Figure 4c). Denotations H and V stand for horizontal and vertical, the light polarization directions in the plane of the paper. For example, $H_{SH}V_F$ represents horizontally polarized second-harmonic (SH) light generated from a vertically polarized fundamental beam. First, let us look at the region at 3–9 o'clock in these SH images. In the $H_{SH}H_F$ image, bright SH signals appear in this region. However, in the $V_{SH}V_F$ image, the signals almost vanish. This means that in this region, strong spontaneous polarization directs in the rubbing direction. On the other hand, in the region at 6–12 o'clock, weak but nonzero SH light can be observed both in the $H_{SH}H_F$ and $V_{SH}V_F$ images at almost the same signal level. This suggests the occurrence of the frustration between the radial growth and the horizontally aligning force by the homogeneous nematic field in this region.

For further discussions, we performed interferometric SHG microscopy (ISHM) to see the directional sense of the polarization more distinctly. The details of the ISHM is described separately in the experimental section. **Figure 5**a shows an $H_{SH}V_F$ ISHM image taken at an arbitrary phase difference of about π

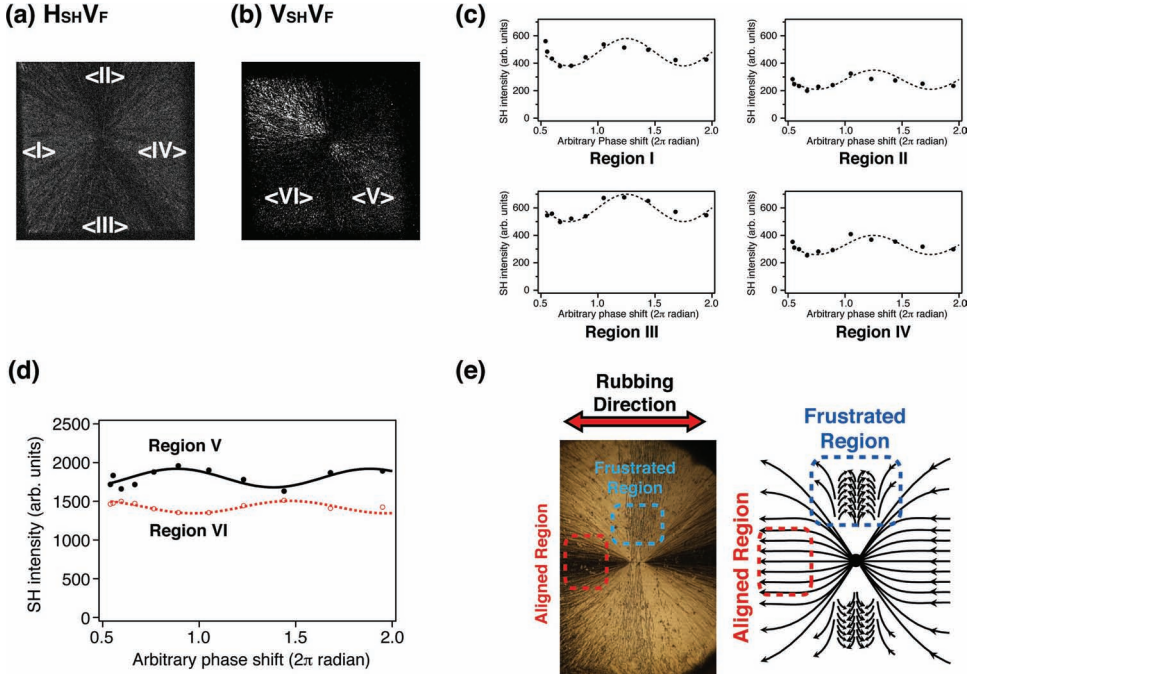

Figure 5. a,b) ISHM images: a) $H_{SH}V_F$ and b) $V_{SH}V_F$ polarization combinations. c,d) Interferometric fringes obtained from: c) regions I–IV in (a) and d) regions V,VI in (b). e) Nanofilament orientations of a <B4/N> domain in a rubbed ultrathin cell. Arrows indicate a distribution of spontaneous polarization directional senses determined from the ISHM images.

radians, giving a mirror symmetric pattern with respect to the axis at 6–12 o'clock and 3–9 o'clock. Plotted in Figure 5c are phase shift dependences of SH signals for four regions I–IV in Figure 5a. All the plots show clear intensity fringes of the same shape. This means that the horizontally-polarized SH signals have the same light phase over the entire image so that the horizontal projection of the spontaneous polarization has the same sense, toward right or left, anywhere in the image. However, $V_{SH}V_F$ ISHM image (Figure 5b) has an asymmetric signal distribution. The regions between 3 and 6 o'clock and between 9 and 12 o'clock show stronger signals than the other regions, whereas the regions between 12 and 3 o'clock and between 6 and 9 o'clock show weaker signals. The stronger and weaker signals mean constructive and destructive interferences. In other words, the vertically polarized SH lights in the former and the latter regions have π-phase-difference, indicating the opposite directional sense in the polarization. This can be more explicitly confirmed by interferometric fringes plotted in Figure 5d which clearly shows π-phase-difference between the regions V and VI in Figure 5b. Therefore, the vertical projections of the spontaneous polarization are opposite in these two regions. Based on these results, we conclude the orientational sense of the polar nanofilaments under the effect of the nematic director field, as illustrated by arrows in Figure 5e. This conclusion also provides the proof that not only the chirality but also the polarity in a single nanofilament domain is preserved in a domain formed from a single nucleus. Indeed, this fact is consistent with the growth model proposed by Chen et al.[14]

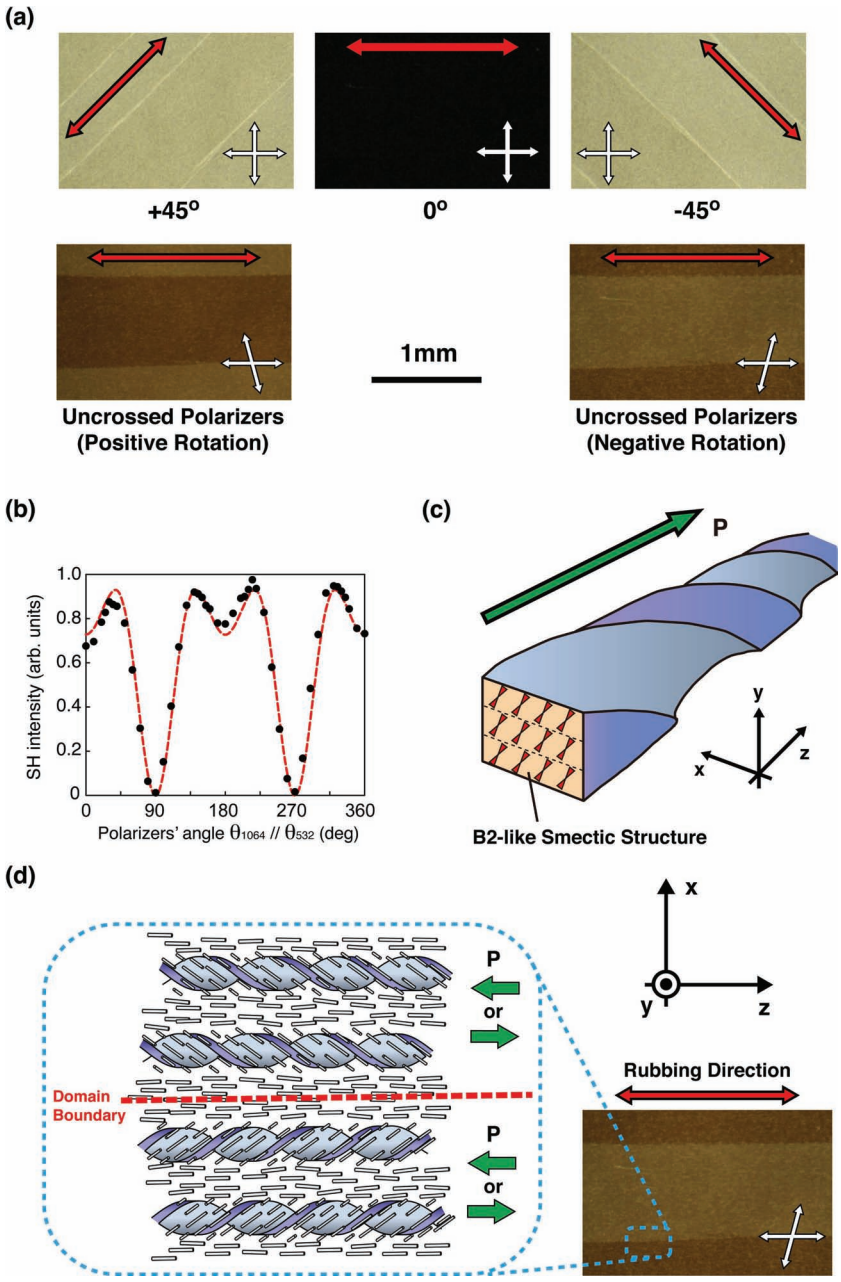

Figure 6. a) POM microscopy images of stripe domains of aligned <B4/N> phase. Red two-way arrows indicate the rubbing direction. b) SH intensity dependence on the polarization angle. c) Assumed local structure of the B4 nanofilament, layered structure of the tilted smectic layers like the B2 phase. d) Plausible model of the aligned nanofilament assembly. One single stripe domain has its own chirality and spontaneous polarization singularity. However, chirality and directional sense of the spontaneous polarization are not correlated. **P** represents a polarization of each filament.

2.3. Enlargement of Aligned Domains

As clearly shown in the previous conclusion, chirality and polar directional sense are unique in a single domain. To further promote and enlarge the uniform nanofilament alignment, we need to restrict the number of nucleation of domains to prevent the coalescence of multiple domains. For the purpose, temperature gradient was introduced along the rubbing direction. The cell was put in a furnace as its edge slightly bumped outside and gently cooled down to <B4/N> from the Iso phase at 1°C/min. Then, the primary nucleation occurred at the edge region, and the nanofilament growth along the rubbing direction was boosted up with the temperature gradient. As a result, we obtained extremely large and uniform chiral domains of several millimeters in length and ≈1 mm in width, as shown in **Figure 6**a. Highly ordered alignment of nanofilaments can be seen as completely dark view under crossed polarizers as shown in the POM image at central top of Figure 6a. The images under uncrossed polarizers (lower right and left in Figure 6a) clearly indicate that the neighboring domains have opposite chirality. Further enlargement of a domain with a single chirality would be possible by

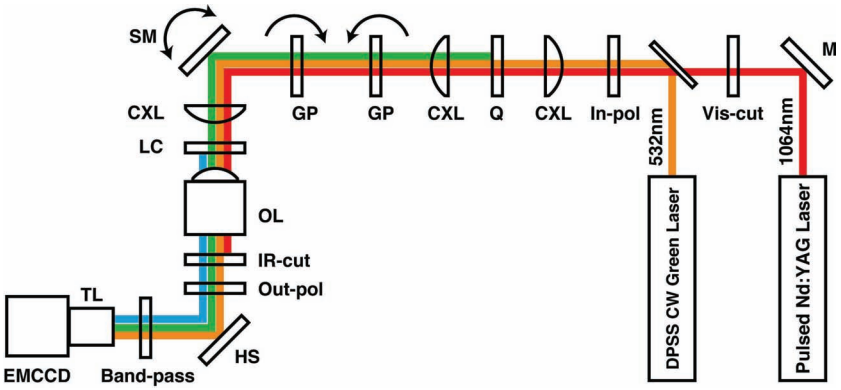

Figure 7. Optical schematic of the ISHM system. M: mirror; Vis-cut: visible-cut glass filter; In-pol: input polarizer; CXL: plano-convex lenses; Q: *z*-cut quartz plate; GP: glass plates; SM: scanning mirror; LC: sample LC cell in a hot stage; OL: long-working distance objective lens (WD 20 mm, 20×, NA 0.40, Mitsutoyo); IR-cut: infrared-red-cut glass filter; Out-pol: output polarizer; HS: harmonic separator; Band-pass: band-pass interference filter; TL: telescopic lens (200 mm, Nikon); EMCCD: cooled electron-magnifying charge coupled device camera (EMCCD). The SH beam from the sample (blue line) interferes with the reference SH beam from the quartz plate (green line) at a certain phase shift induced by two counter-rotating glass plates. Counter-rotation of two glass plates compensates the spatial drift of the beam.

properly designing the temperature gradient. The investigation is under way. We want to emphasize that comparing with the method previously proposed by Yoon et al.,[10] the present method is suitable to obtain a larger single domain and much simpler because of the use of self organization of LCs.

At last, more quantitative SHG analysis was made for these stripe domains of the aligned nanofilament in the <B4/N> state to confirm their uniformity. The result is shown in Figure 6b together with a theoretical fitting. Because of the use of an ultrathin cell, birefringence and optical activity are ignored in this theoretical calculation. Besides, the present experimental geometry (normal beam incidence) does not allow any chiral nonlinear optical effect in this experiment, so that imaginary contribution such as magnetic components is not taken into account in the nonlinear susceptibility χ, differently from our previous study.[17] From the best fit for the experimental result (red broken curve in Figure 6b), the ratio of effective nonlinear susceptibility tensor components was obtained as χ_{333}/χ_{311} = 1.41, where subscripts 1 and 3 correspond respectively to *z*- and *x*-axes in the coordinates indicated in Figure 6. Nonlinear optical properties of the B2 phase have already been studied well in our previous report, where χ_{333}/χ_{311} = 0.29.[18] The main reason of the five times difference is, probably, smaller χ_{311} value in the <B4/N> state. The B4 nanofilament has locally the tilted layer structure like a B2 phase and forms a helix.[6,10,14,19] In each single helical nanofilament, the molecular bent direction, i.e., polar direction, is considered to be aligned uniformly along the helical axis (*z*-axis) as shown in Figure 6c. Therefore, χ_{333} is essentially the same in B2 and B4, whereas some extent of cancellation may occur in χ_{311} about the helical axis. The same SHG measurement was conducted for several points in the same domain, and the good experimental reconstructivity was confirmed. So in each large single chiral stripe domain, helical nanofilament assemblies are considered to be in highly ordered state with uniform polarity as depicted in Figure 6d. However, polarity and chirality in each single domain are uncorrelated and hence independent from each other. These results are very interesting from the viewpoint of material science to gain uniform macroscopic materials with spontaneously symmetry-broken structure, offering attractive possibilities for novel optical/electronic materials such as for nonlinear optics, piezoelectric elements, etc.

3. Conclusions

We prepared a new binary mixture system of bent-shaped (P-8-OPIMB) and rod-shaped (5PCB) LCs for the sake of alignment control of the B4 helical nanofilament assembly. SH microscopy and interferometric SH microscopy were carried out to study the internal polar structure of the helical nanofilment domains of this mixture. Alignment control of the B4 helical nanofilament assembly by the nematic director field of 5PCB was successful. The aligned nanofilament domains appear as smooth and uniform stripes over millimeters. SHG measurement and analysis revealed that in these aligned domains, polarity was preserved from the nucleus, as well as chirality. Such an eccentric nanoassembly may not merely be attractive as a scientific subject but also suggests a novel approach for tailoring functional bulk materials.

4. Experimental Section

Sample Preparation: Weighed compounds P8 and 5PCB were dissolved together in chloroform, and mixed well with sonication. Afterwards, the mixture was dried up thoroughly by heating to remove the solvent. Three types of cells with quartz substrates coated with polyimide alignment films (AL1254, JSR) were prepared: a) 5-μm-thick cell without rubbing for polarizing microscopy, b) ultrathin cell (several-hundreds-nm-thick) without rubbing for CD measurements, and c) ultrathin cell with antiparallel rubbing for alignment experiments. The ultrathin cells were sandwich-shaped ones consisting of two smooth fused-silica substrates, fabricated without spacers. Cell gaps were estimated by optical simulation (SCOUT, W. Theiss Hard- and Software) upon transmittance spectrum measurement with a multichannel monochromator (USB4000, Ocean Optics) and a polarizing optical microscope (OPTIPHOT-POL, Nikon).

Circular Dichroism Measurement: For CD measurements, a focal reducing optics was built up in the optical path in a commercial CD spectrometer (J-720WI with an OR optional unit, JASCO) to detect the signal from a small region. The detailed schematic is shown in ref. [8].

Interferometric Second-Harmonic Generation Microscopy: ISHM is a technique based on SHG microscopy combined with SHG interferometry.[20] As shown in Figure 4a,b, conventional SHG microscopy can resolve the distribution of polar domains and their orderings. On the other hand, SHG interferometry can probe the relative directional sense of the polar specimen, so that be commonly used to judge the polarization reversal in ferroelectric LCs.[21,22] Hence, ISHM can visualize the directional sense of the polar domains. **Figure 7** is the optical configuration of the ISHM. The polarized fundamental beam of 1064 nm light pulses from a high-repetition-rate Q-switched neodymium-yttrium-garnet laser (Nd:YAG, 100 Hz, BM Industries 501-D.NS4/100) was first focused onto a *z*-cut quartz plate to generate a reference

SH beam. The residual fundamental and the reference SH beams are collimated and then led through two counter-rotating optical-graded glass plates. Thus, because of the refractive index dispersion of glass, a phase shift is introduced between the fundamental and the reference SH beams by rotating the glass plates. Then the beams are focused again on the sample plane. Consequently, an SH beam generated from the sample interferes constructively or destructively with the reference SH beam, depending on the directional sense of the sample and the phase shift. The resulted interferometric SH signal was analyzed by an output polarizer, qualified with optical filters, expanded with a telescopic lens, and finally taken by a cooled electron-multiplying charge-coupled device camera (EMCCD, iXon, Andor Technology) as a wide-field image. Such a highly sensitive wide-field detector device is very useful to detect wide-field SH images. However, since the interferometric condition is so severe in the ISHM technique, wide-field illumination, which often gives speckle noises on the image, is not favorable. Therefore, in our setup, the beams are tightly focused on the sample. Instead, wide-field scanning by a mechanical mirror was carried out during the camera's exposure. A green continuous light beam from a diode-pumped Nd:YAG laser was used as a guide beam for optical alignment and also used as a light source for taking real images.

Received: July 9, 2012
Published online: January 11, 2013

[1] T. Niori, T. Sekine, J. Watanabe, T. Furukawa, H. Takezoe, *J. Mater. Chem.* **1996**, *6*, 1231.
[2] H. Takezoe, Y. Takanishi, *Jpn. J. Appl. Phys.* **2006**, *45*, 597.
[3] D. R. Link, G. Natale, R. Shao, J. E. Maclennan, N. A. Clark, E. Korblova, D. M. Walba, *Science* **1997**, *278*, 1924.
[4] T. Sekine, Y. Takanishi, T. Niori, J. Watanabe, H. Takezoe, *Jpn. J. Appl. Phys.* **1997**, *36*, L1201.
[5] T. Sekine, T. Niori, M. Sone, J. Watanabe, S.-W. Choi, Y. Takanishi, H. Takezoe, *Jpn. J. Appl. Phys.* **1997**, *36*, 6455.
[6] L. E. Hough, H. T. Jung, D. Kruerke, M. S. Heberling, M. Nakata, C. D. Jones, D. Chen, D. R. Link, J. Zasadzinski, G. Heppke, J. P. Rabe, W. Stocker, E. Korblova, D. M. Walba, M. A. Glaser, N. A. Clark, *Science* **2009**, *325*, 456.
[7] T. Otani, F. Araoka, K. Ishikawa, H. Takezoe, *J. Am. Chem. Soc.* **2009**, *131*, 12368.
[8] F. Araoka, G. Sugiyama, K. Ishikawa, H. Takezoe, *Opt. Mater. Express* **2011**, *1*, 27.
[9] C. Zhu, D. Chen, Y. Shen, C. D. Jones, M. A. Glaser, J. E. Maclennan, N. A. Clark, *Phys. Rev. E* **2010**, *81*, 011704.
[10] D. K. Yoon, Y. Yi, Y. Shen, E. D. Korblova, D. M. Walba, I. I. Smalyukh, N. A. Clark, *Adv. Mater.* **2011**, *23*, 1962.
[11] J. W. Goodby, *Curr. Opin. Solid State Mater. Sci.* **1999**, *4*, 361.
[12] T. Kato, *Science* **2002**, *295*, 2414.
[13] V. Percec, M. Glodde, T. K. Bera, Y. Miura, I. Shiyanovskaya, K. D. Singer, V. S. K. Balagurusamy, P. A. Heiney, I. Schnell, A. Rapp, H.-W. Spiess, S. D. Hudson, H. Duan, *Nature* **2002**, *417*, 384.
[14] D. Chen, J. E. Maclennan, R. Shao, D. K. Yoon, H. Wang, E. Korblova, D. M. Walba, M. A. Glaser, N. A. Clark, *J. Am. Chem. Soc.* **2011**, *133*, 12656.
[15] I. Drevensek Olenik, R. Torre, M. Copic, *Phys. Rev. E* **1994**, *50*, 3766.
[16] M. I. Barnik, L. M. Blinov, A. M. Dorzhkin, N. M. Shtykov, *Mol. Cryst. Liq. Cryst.* **1983**, *98*, 1.
[17] F. Araoka, N. Y. Ha, Y. Kinoshita, B. Park, J. W. Wu, H. Takezoe, *Phys. Rev. Lett.* **2005**, *94*, 137801.
[18] F. Araoka, J. Thisayukta, K. Ishikawa, J. Watanabe, H. Takezoe, *Phys. Rev. E* **2002**, *66*, 021705.
[19] F. Araoka, T. Otani, K. Ishikawa, H. Takezoe, *Phys. Rev. E* **2010**, *82*, 041708.
[20] J. Kaneshiro, S. Kawado, H. Yokota, Y. Uesu, T. Fukui, *J. Appl. Phys.* **2008**, *104*, 054112.
[21] M. Nakata, D. R. Link, F. Araoka, J. Thisayukta, Y. Takanishi, K. Ishikawa, J. Watanabe, H. Takezoe, *Liq. Cryst.* **2001**, *28*, 1301.
[22] D. Miyajima, F. Araoka, H. Takezoe, J. Kim, K. Kato, M. Takata, T. Aida, *Science* **2012**, *336*, 209.